Estimation of Two-Dimensional Joint Stiffness Matrices Using Vibration Experiments

Undergraduate Honors Thesis

Presented in Partial Fulfillment of the Requirements for
Graduation with Distinction in the
Department of Mechanical Engineering at
The Ohio State University

By:

Ron Taulbee

Advisor: Dr. Rajendra Singh

Co-Advisor: Dr. Jason Dreyer

****

The Ohio State University

November 2011

Defense Committee:

Dr. Rajendra Singh
Dr. Jason Dreyer
Dr. Robert Siston

Abstract

Multi-directional stiffness matrices of elastic joints, such as elastomeric bushing in automotive suspensions, are not easily quantified and are often simplified as diagonal matrices, ignoring effects of coupling among the different directions contained in off-diagonal terms in the matrices. The purpose of this study is to examine two procedures to quantify the complete two-dimensional stiffness matrices of different elastic joints. The procedures are both based on dynamic measurements on a rigid body with well-known inertia properties supported by a flexible joint with known center of motion. The first method uses the known inertia properties, measured resonant frequencies and the corresponding mode shapes of the system to calculate the stiffness matrix of the joint. The second method directly calculates the stiffness matrix using the known inertia properties and accelerance measurements collected over a range of frequencies. A controlled experiment with a system with known stiffness matrix, kinetic constraints, and inertia properties was created. Using accelerances from impulse hammer measurements, a unique stiffness matrix was obtained for a variety of joints and analyzed using each method. The sources of error are discussed along with ways in which to potentially minimize the effects of these errors.

Table of Contents

Acknowledgements

I would like to thank all the people that have provided help and support over the course of this project. I am thankful for the guidance offered by both Dr. Rajendra Singh and Dr. Jason Dreyer. I would also like to thank all the students and resources in the Acoustics and Dynamics Laboratory at The Ohio State University. This project would not have been possible without the facilities provided by the Department of Mechanical and Aerospace Engineering throughout Scott Lab. Finally special thanks go to the National Science Foundation for providing funding for this project through the Research Experiences for Undergraduates Grant as well as to the NSF Center in Smart Vehicle Concepts at The Ohio State University.

Table of Figures

Chapter 1: Introduction

1.1 Background

A common application of bushings is their use in the automotive industry to reduce noise, vibration, and harshness (NVH) generated from the loadings on the wheels or body of the car that is transferred to the passenger through the steering wheel or seat track. This requires a trade-off in terms of ride quality and vehicle responsiveness as "softer" bushings are better for vibration control but reduce the handling of the vehicle. Though bushings are utilized in many applications, their static and dynamic behavior is poorly understood. If an accurate model of the bushings under multi-dimensional loading were available, these components could be designed in such a way to greatly mitigate the noise and vibration problems while maintaining the desired vehicle control.

Due to the lack of understanding in the multi-dimensional properties of bushings, the bushing is normally rated for loading in only one direction, or possibly up to two directions with the second direction being a static load only. This practice is viewed as acceptable across the industry because bushings are primarily used to reduce vibrations along only a certain axis of the bushing. Ideally, a bushing would be used in a situation where all the forces experienced by the bushing were in the direction that it is rated for, but in all practical applications the bushing will experience forces and moments in all directions. Figure 1.1 shows such an application, where the bushings are used to control vibrations between the lower control arm and the frame of a car. With the wheel experiencing forces in all directions from the road, it can be seen that the bushings will experience forces and moments in all directions as well.

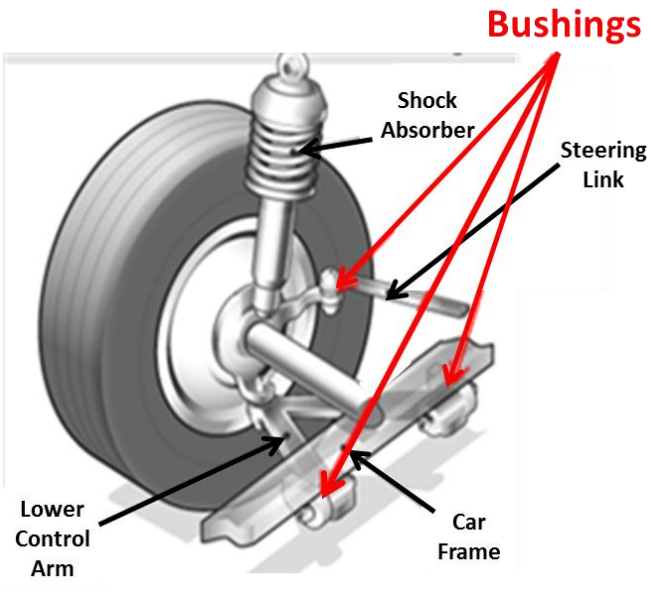

Figure 1.1: Automotive Bushings on Lower Control Arm
(adapted from auto.howstuffworks.com)

For the sake of illustration, consider three forces and three moments leading a stiffness matrix of dimension six. Figure 1.2 displays this model of a standard bushing with the six degrees of freedom.

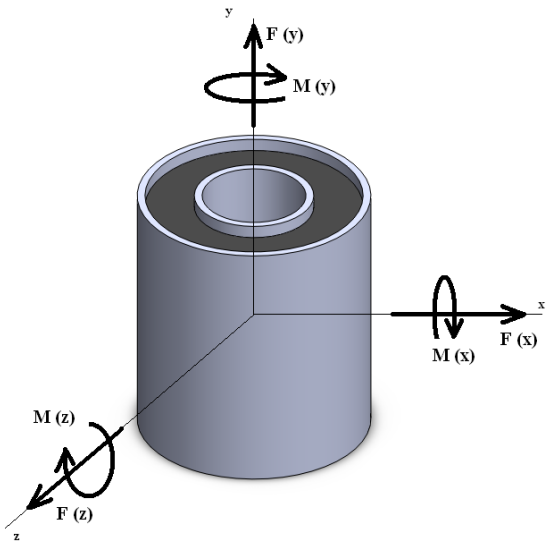

Figure 1.2: Bushing Under Multi-Dimensional Loading

1.2 Literature Review

Many tests have been developed to effectively measure how a bushing reacts under a single load and can be used to measure the stiffness and damping values of the bushing in the direction being tested [1]. These machines are widely used throughout industry but are developed only to measure the bushing properties in one direction, possibly two, and are thus incapable of completely defining the stiffness properties of the bushing in all six degrees of motion.

Literature reveals many mathematical approaches that have been utilized in an attempt to describe the motion of bushings. Analyzing a bushing in one direction, the system can be effectively modeled using Kelvin-Voigt formulation which treats the material as a dynamic system consisting of a purely elastic spring (stiffness) and a purely viscous damper (damping) connected in parallel [2]. Figure 1.3 shows a bushing with an applied static mean load as well as a dynamic sinusoidal displacement excitation along a single axis and the equivalent linear system derived by applying a simplified Kelvin-Voigt model.

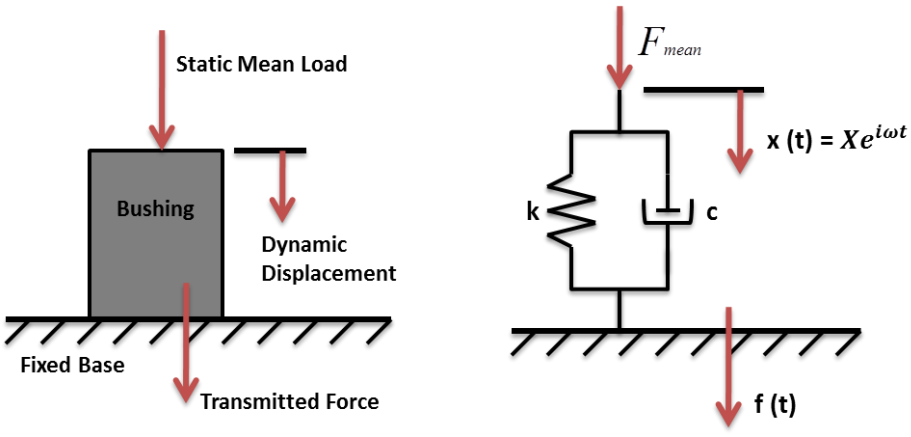

Figure 1.3: Kelvin-Voigt Formulation for Bushing in One Direction

Measuring the transmitted force through the fixed base, the force component can be found and can then be used to represent the dynamic stiffness and damping values of the bushing in terms of complex stiffness magnitude and loss angle [1,3]. The resulting stiffness and damping properties will be represented by real and imaginary components which represent both dissipative and storage components of the complex stiffness. The problem, however, is that this model only applies to a uni-axial case. For loading applied in multiple directions on the bushing, a Kelvin-Voigt model in each direction would need to be applied, resulting in multiple springs and dampers connected in series and parallel, creating a more complex model. Also by fixing a boundary condition as seen in Figure 1.3, the motion of the system will be restricted and thus other mathematical formulations must be utilized in characterizing the multi-dimensional properties.

Several mathematical approaches, including nonlinear finite elements and empirical dynamics methodology [3-6], have also attempted to determine how a bushing acts under certain loading conditions, all requiring the use of some kind of experimental data input. The physical meaningfulness of these models however, has yet to be verified. In calculating the stiffness matrix of the system, there are an infinite number of different matrices that will produce the same behavior of any system. Such models [3-6] do not determine or account for a unique solution to the stiffness of a particular system.

Literature also introduces the notion of a stiffness matrix which can be used to fully describe the stiffness properties of a system [7]. A stiffness matrix contains stiffness values in each direction of motion that the system is free to move in and includes coupling coefficients representing the relationships between the stiffness properties in different directions. These coupling coefficients are represented by the off-diagonal terms in the stiffness matrix. If the off-

diagonal terms are all equal to zero, there is no coupling in the system and the directions of motion are uncoupled. These coupling terms are also proven to be dominant in some systems and must be investigated.

A method that can theoretically be used to determine the multi-axial stiffness matrix of a joint using rigid-body dynamics has been previously developed [8]. This method claims that acceleration data, measured from experiment, can be related to a pivot point from which the reaction forces and the relative displacements about the pivot point can be calculated. Using these calculated values, the multi-dimensional stiffness matrix can then be derived. This method of determining joint stiffness has been tested on applications involving power tools but lacks experimental validation through theoretical comparison. The mathematics behind this joint stiffness calculation method are explained more thoroughly in Chapter 3.

1.3 Project Objective

In looking for a way in which to determine the stiffness properties of bushings, this study aims to experimentally validate previously developed methods of calculating multi-directional stiffness properties on elastic joints. Two methods in particular are to be examined. One is a resonance-based calculation that requires determination of the resonant frequencies and mode shapes from which the stiffness properties can be derived. The second method tested is the joint stiffness measurement, based on measured multi-dimensional rigid body motions [7]. An experiment is to be designed such that each of these methods can be applied to determine the stiffness matrix of a system which can also be determined theoretically for comparison purposes. The goal is to establish an experimentally validated procedure which can be followed to determine a unique stiffness matrix of a multi-dimensional system. To accomplish this goal, the specific objectives of this research are as shown:

1) Design a simplified experiment such that the stiffness of the system can be theoretically calculated as well as measured using methods for stiffness calculation based on rigid-body dynamics
2) Experimentally validate two methods of determining multi-dimensional stiffness matrices by comparing measured stiffness values to values calculated based on theory
3) Determine if either method can be used to measure a unique stiffness matrix of a multi-degree of freedom system

By designing an experiment from which the stiffness matrix can be measured and theoretically calculated, the values can be compared and used to evaluate the assumptions and error in the experimental setup. The assumptions that are made include no/proportional damping in the system, a constant center of rotation, and simplified two degree of freedom motion, as well as other measurement based assumptions as will be explained throughout.

Chapter 2: Experiment

2.1 Two Degree of Freedom System Model

To verify the procedures for determining the multi-directional stiffness matrix, modal impact testing was performed on a two degree of freedom system, modeled as shown in Figure 2.1. This was done to obtain the frequency response functions (FRFs) of the system, from which the natural frequencies and mode shapes could be estimated. A simple two degree of freedom system was used in the experiment so that the measured values could be compared to the analytical solution determined mathematically using a limited number of variables.

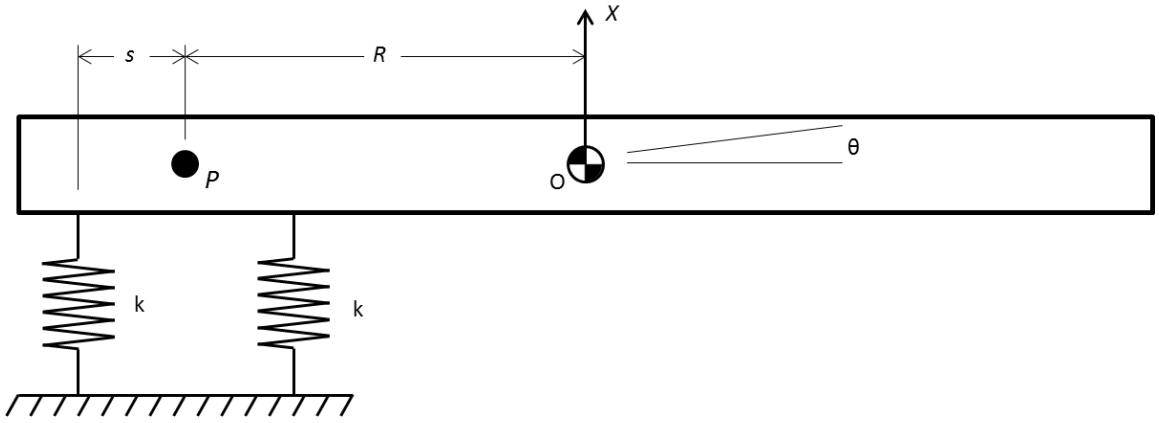

Figure 2.1 Two Degree of Freedom System with Mass and Two Springs

As shown in Figure 2.1, *x* represents the translational motion of a rigid beam in the direction shown and θ represents the rotational motion about the *z* axis. Point *O* represents the center of mass of the beam and point *P* is the elastic center of the beam. The beam has a mass of *m* and a mass moment of inertia about the center of mass equal to I_o. The center of rotation is assumed to be the location of the elastic center and the distance between the center of rotation and each spring is *s* as shown in the figure. The distance then from the center of mass to the center of rotation is denoted by *R*.

When the system is excited the beam will rotate as well as move in the *x* direction and the free body diagram will look like that shown in Figure 2.2.

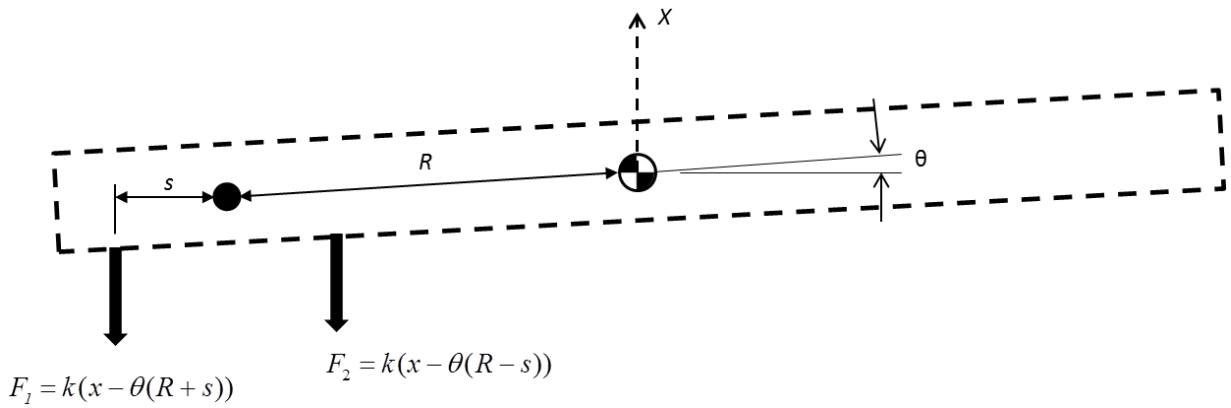

Figure 2.2: Free Body Diagram of Two Degree of Freedom System at Mass Center

The two forces represent the forces applied to the beam by the springs as a result of their stretching. These will be the only forces acting on the system because the excitation force is a driving point impulse excitation and not a continuously applied force. The total deflection of each spring will be dependent on the translational motion of the beam as well as the rotation and the forces can be modeled as shown in Figure 2.2. Small angle approximations are used in determining these forces and are used in the following calculations as the deflections of the beam are nominally small. With the equations for the spring forces known, force and moment summations can be performed on the free body diagram with results as shown:

$$m\ddot{x} + 2kx - 2kR\theta = 0 \qquad \textbf{(1)}$$

$$I_0\ddot{\theta} - 2kRx + (2kR^2 + 2ks^2)\theta = 0 \qquad \textbf{(2)}$$

By then taking Equations 1 and 2 and putting them into matrix form the resultant equation is shown in Equation 3.

$$\begin{bmatrix} m & 0 \\ 0 & I_o \end{bmatrix}\begin{bmatrix} \ddot{x} \\ \ddot{\theta} \end{bmatrix}+\begin{bmatrix} 2k & -2kR \\ -2kR & (2kR^2+2ks^2) \end{bmatrix}\begin{bmatrix} x \\ \theta \end{bmatrix}=\begin{bmatrix} 0 \\ 0 \end{bmatrix} \quad \textbf{(3)}$$

Equation 3 can then be used to describe **M** and **K** which represent the effective mass matrix and effective stiffness matrix respectively.

$$\mathbf{M}=\begin{bmatrix} m & 0 \\ 0 & I_O \end{bmatrix} \qquad \mathbf{K}=\begin{bmatrix} k_{x,x} & k_{x,\theta} \\ k_{\theta,x} & k_{\theta,\theta} \end{bmatrix}=\begin{bmatrix} 2k & -2kR \\ -2kR & (2kR^2+2ks^2) \end{bmatrix} \quad \textbf{(4)}$$

It can be seen in Equation 4 that the mass matrix is diagonal while the stiffness matrix is not. This form is characteristic of the case where the system of equations is derived about the center of mass of the system resulting in a diagonal mass matrix. Equation 4 also shows the representation of the stiffness matrix, **K**, in terms of the individual stiffness components where the diagonal terms describe the stiffness values in purely one direction and the off-diagonal terms represent the coupling effects between the different directions.

The system can be described by an infinite number of equivalent systems of matrices. An alternate example can be seen by the case where the motion is described by moving the translational *x* direction to the center of rotation as shown in Figure 2.3.

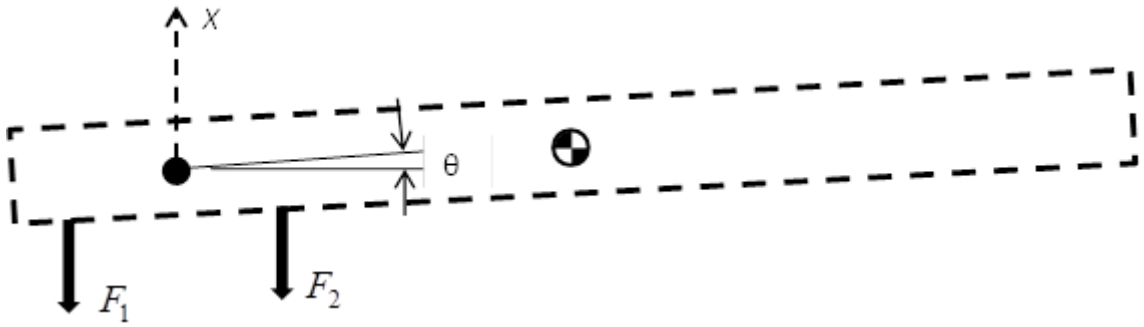

Figure 2.3: Free Body Diagram of Two Degree of Freedom System at Center of Rotation

Again force and moment summations are performed and with the use of the parallel axis theorem, the system of equations, in matrix form is as shown in Equation 5.

$$\begin{bmatrix} m & mR \\ mR & (I_o + mR^2) \end{bmatrix} \begin{bmatrix} \ddot{x} \\ \ddot{\theta} \end{bmatrix} + \begin{bmatrix} 2k & 0 \\ 0 & 2ks^2 \end{bmatrix} \begin{bmatrix} x \\ \theta \end{bmatrix} = \begin{bmatrix} 0 \\ 0 \end{bmatrix} \quad \textbf{(5)}$$

Here it can be seen that the stiffness matrix is diagonal while the mass matrix is not. The diagonal stiffness matrix is characteristic of the case where the system of equations is determined at the elastic center of the system. While these mass and stiffness matrices are not equal to the ones derived in Equation 4, they represent equivalent systems and will have the same natural frequencies and mode shapes. To stay consistent throughout, the mass and stiffness matrices from Equation 4 will be used in all following calculations.

Using a low order system will provide more insight into the effects of each value on the stiffness of the system, due to the fact that the equations can be written analytically in terms of a few variables. With the mass and stiffness matrices defined, shown by Equation 4, the mode shapes and frequencies of the system are determined by finding the eigenvalues of the system. The first step in the process of determining the frequencies and mode shapes is to realize that Equation 3 represents the two degree of freedom form of the general equation of undamped free vibration as shown in Equation 6:

$$\mathbf{M}\ddot{\mathbf{x}} + \mathbf{K}\mathbf{x} = 0 \quad \textbf{(6)}$$

By assuming that the solutions of Equation 6 are periodic, due to either proportional damping or the lack of damping, the normal-mode solution can be described using the frequency data of the response. The generalized solution to Equation 6 will take the form of Equation 7.

$$\mathbf{x}(t) = \mathbf{X}e^{i\omega t} \qquad (7)$$

In Equation 7, ω represents the frequency of vibration in units of radians per second and **X** is the vector of amplitude constants called the mode shape. Realizing that the exponential part of the solution is non-zero for all time values, Equation 7 substituted into Equation 6 results in Equation 8.

$$\left(-\omega^2\mathbf{M}\mathbf{X} + \mathbf{K}\mathbf{X}\right)e^{i\omega t} = 0 \qquad -\omega^2\mathbf{M}\mathbf{X} + \mathbf{K}\mathbf{X} = 0 \qquad (8)$$

Because the mass matrix is nonsingular, Equation 8 can be pre-multiplied by the inverse of the mass matrix resulting in Equation 9 which is of the form to be solved for the eigenvalues and the resultant eigenvectors.

$$\left(\mathbf{M}^{-1}\mathbf{K} - \omega_r^2\mathbf{I}\right)\mathbf{X} = 0 \qquad (9)$$

The eigenvalues of the system will represent the frequencies, ω_r, for which Equation 9 is satisfied, and the resultant eigenvectors, **X**, at these frequencies are the mode shape vectors of the system. Equation 10 shows the resultant eigenvalue equation derived from Equation 9. The solution to the eigenvalue problem will then consist of the $\mathbf{\Omega}^2$ and **V** matrices containing the resonant frequencies and mode shapes of the system respectively as shown in Equation 11.

$$\mathbf{M}^{-1} \cdot \mathbf{K} \cdot \mathbf{V} = \mathbf{V} \cdot \mathbf{\Omega}^2 \qquad (10)$$

$$\mathbf{\Omega}^2 = \begin{bmatrix} \omega_1^2 & 0 \\ 0 & \omega_2^2 \end{bmatrix} \qquad \mathbf{V} = \begin{bmatrix} X^{(1)} & X^{(2)} \\ \theta^{(1)} & \theta^{(2)} \end{bmatrix} \qquad (11)$$

2.2 Experimental Realization

An experiment was designed to model the two degree of freedom system, shown in Figure 2.1, by connecting a steel beam to a fixed clamp using four identical springs. Impact testing was performed with two accelerometers and an impulse hammer as shown in Figure 2.4.

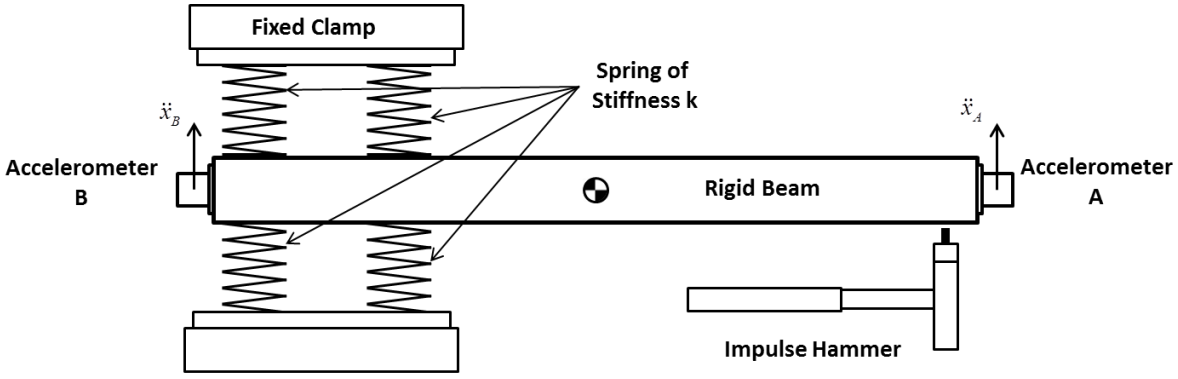

Figure 2.4: Experimental Setup for Two Degree of Freedom System

The accelerometers used were PCB 356115 tri-axial, piezo-electric accelerometers (although only one axis of each accelerometer was used). Both accelerometers were calibrated using a calibrated shaker (PCB Model 394C06) to determine the actual sensitivities. The accelerometer marked as accelerometer A in Figure 2.4, serial number 10347, was determined to have a sensitivity of 102 mV/g. Accelerometer B, serial number 10366, was measured to have a sensitivity of 94 mV/g. The system was excited with a PCB 086C02 impulse hammer, serial number 21828, with a sensitivity rating of 11.2 mV/N. The two accelerometers and the impulse hammer were connected to an NI Compact DAQ setup with a 9234 module (24 bit +/- 5 V Simultaneously Sampled Analog Input with Piezoelectric Conditioning). The sampling parameters were set to a force-exponential window with a sampling frequency of 1652 Hz with 1024 data points measured and five averages were taken at each impact location. The five averages were taken in an attempt to reduce bias error. The data was collected using NI

SignalExpress and analyzed using Matlab software. A measurement-based assumption was made that the accelerometers used in the experiment were phase matched across the frequency range of interest. If the accelerometers are not phase matched, then another source of error in introduced.

The rigid beam that was used in this experiment was a rectangular A36 steel beam; twelve inches in length, two inches wide, and one inch thick (0.3048 m x 0.0508 m x 0.0254 m). Four compression springs were connected to the beam and to a fixed clamp to allow the system to oscillate with minimal damping. Each spring was measured to have a diameter of 1.375 inches (0.0349 m) and the stiffness value for each was determined by loading the springs, with a known force, and measuring the static deflection. The stiffness of each spring was calculated to be 21.9 N/mm. The springs were aligned so that two springs would be in parallel and the system could be modeled as shown in Figure 2.1. With the springs modeled in parallel, each of the two springs then had an effective stiffness of 43.8 N/mm.

To test multiple systems and observe changes in stiffness values between the systems, six different setups were analyzed by changing the locations of the springs. For three of the experimental systems, one spring was attached at the end of the beam and the other spring was placed at varying distances between the first spring and the center of mass of the beam. Figure 2.5, Figure 2.6, and Figure 2.7 show these systems where the distances between the springs are 0.5 inches (0.0127 m), 1.5 inches (0.0381 m), and 2.5 inches (0.0635 m) respectively. The distances are measured between the outer diameters of the springs as shown.

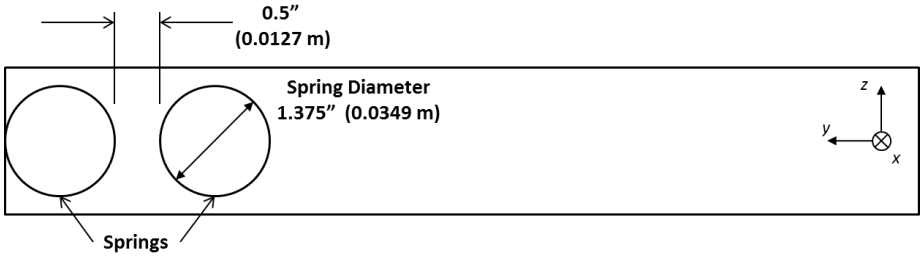

Figure 2.5: Spring Locations for Experimental Configuration 1

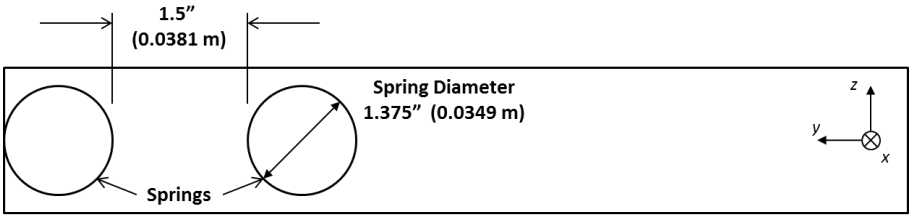

Figure 2.6: Spring Locations for Experimental Configuration 2

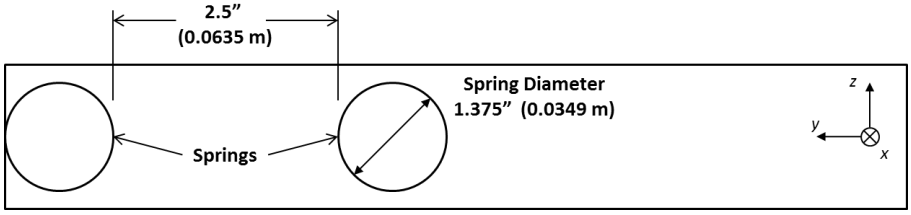

Figure 2.7: Spring Locations for Experimental Configuration 3

The other three experimental systems were configured by varying the distance between the springs, while keeping them centered about the beam’s center of mass. Again the distances between the springs are 0.5 inches (0.0127 m), 1.5 inches (0.0381 m), and 2.5 inches (0.0635 m) as shown in Figure 2.8, Figure 2.9, and Figure 2.10 respectively.

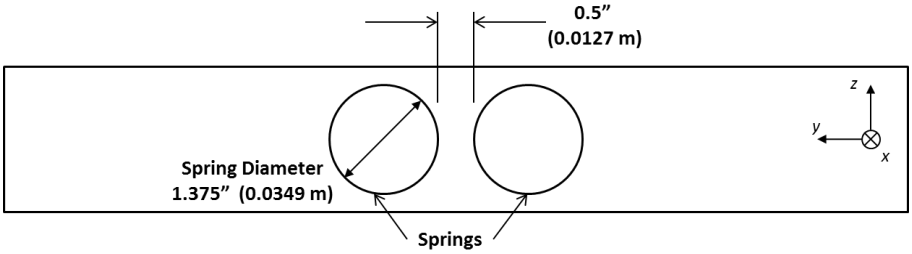

Figure 2.8: Spring Locations for Experimental Configuration 4

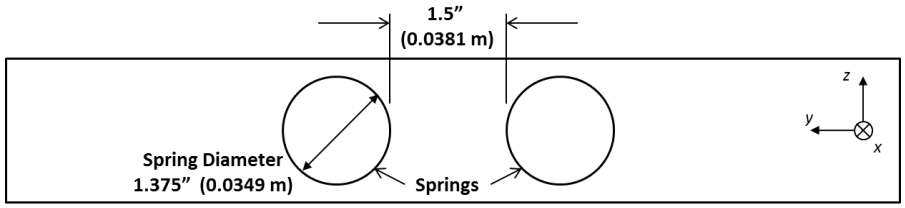

Figure 2.9: Spring Locations for Experimental Configuration 5

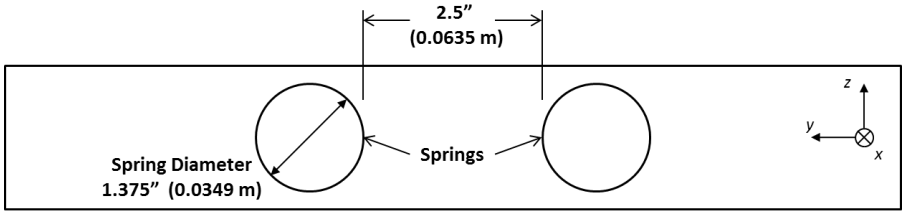

Figure 2.10: Spring Locations for Experimental Configuration 6

The system was excited by hitting it with the impulse hammer on the end of the beam and the two accelerometers recorded the accelerance data at each end of the beam as it oscillated. With an accelerometer located on each end of the beam, the motion of the system in both the translational direction and the rotational direction could be measured. Impact testing was chosen for the experiment so that accelerance data could be obtained for use in both methods of stiffness calculation as will be described. By using impact testing, the system is excited at all frequencies, observable at the driving point in the x-y plane, so that the resonant frequencies do not have to be calculated prior to testing. From the accelerance spectra measurements, the quadrature spectra of each system are plotted and these are used to obtain the resonant frequencies and mode shapes of the systems.

Chapter 3: Method of Procedure

3.1 Resonant Method

3.1.1 Method Description

The first method examined uses the mode shapes and frequencies, measured from the imaginary components of the accelerance measurements, to calculate the stiffness matrix of the system. When the mass and stiffness matrices are known, the mode shapes and frequencies are calculated by finding the eigenvalues of the system as shown in Equation 10. However, if the resonant frequencies are measured and used to fill the diagonal $\mathbf{\Omega}^2$ matrix and the mode shape vectors are measured at these frequencies and used to fill the **V** matrix, then the eigenvalue decomposition can be solved to obtain the stiffness matrix. Equation 10 can be solved for **K** and Equation 12 represents the final equation used in calculating the stiffness matrix of a system with a known mass matrix, after the modes and frequencies of the system have been measured. In Equation 12, **U** is the normalized mode shape matrix.

$$\mathbf{K} = \mathbf{M} \cdot \mathbf{U} \cdot \mathbf{\Omega}^2 \cdot \mathbf{U}^{-1} \qquad \textbf{(12)}$$

To measure the modes and frequencies used in Equation 12, the frequency responses must be obtained and from these the quadrature spectra, which are the imaginary components of the accelerance measurements, are plotted. From the quadrature spectra plots, the natural frequencies of the system are determined by finding the frequencies at which the system experiences resonance, shown by the peaks in the response. The mode shapes are then calculated indirectly from the frequency response plots by finding the peak values of the normalized amplitude, measured at each of the resonant frequencies. Figure 3.1 shows a schematic of an example quadrature spectra plot that may be obtained for a two degree of freedom system. This

plot is shown for demonstration purposes only and does not reflect any of the experimental results obtained.

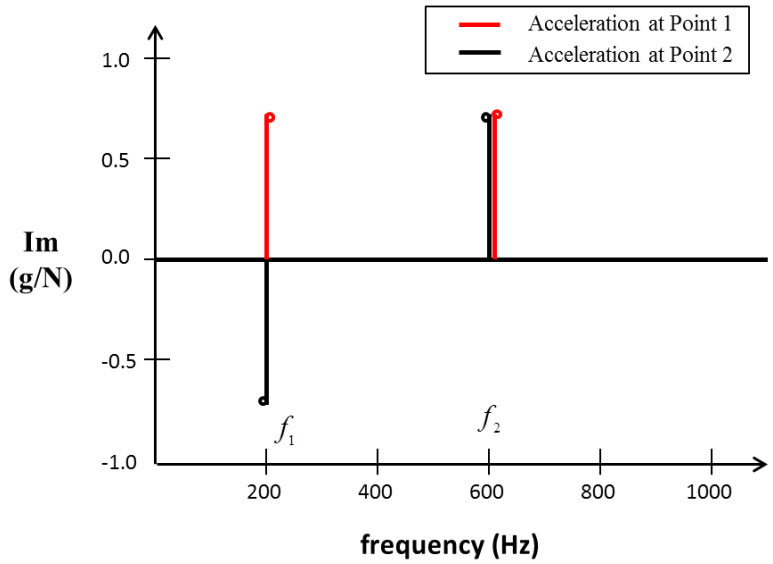

Figure 3.1: Schematic of Example Quadrature Spectra Plot

From Figure 3.1 it can be seen that the resonant frequencies of the example system would be the frequencies marked by f_1 and f_2, corresponding to approximately 200 and 600 Hertz (Hz). At each of the resonant frequencies, the normalized amplitude values are recorded for each point and these are used to determine the mode shapes of the system. In Figure 3.1 these values are measured to be roughly 0.7 and -0.7 for locations 1 and 2 respectively at 200 Hz and 0.7 for both locations at 600 Hz.

The procedure for calculating the mode shapes from these amplitude readings will be dependent on the kinematics of the system and it is in this step that it becomes significantly more difficult to use this method for calculating stiffness matrices of systems with higher degrees of freedom, as will be illustrated. From the frequency response, the measured amplitudes represent the acceleration values at each accelerometer location and these measurements need to be converted into values that represent the motion of the system in terms of x and θ. This is done for

the two degree of freedom system shown in Figure 2.1 by first transforming the acceleration measurements into the frequency domain and solving for the displacements as shown in Equation 13.

$$\begin{bmatrix} x_i(\omega) \\ x_j(\omega) \end{bmatrix} = -\frac{1}{\omega^2}\begin{bmatrix} \ddot{x}_i(\omega) \\ \ddot{x}_j(\omega) \end{bmatrix} \quad \textbf{(13)}$$

In Equation 13, x_i represents the displacement of the accelerometer shown as accelerometer A in Figure 2.4 and x_j represents the displacement of the accelerometer shown as accelerometer B. Using these displacement measurements and the geometry of the system the motion can be described in terms of *x* and θ as shown in Equations 14 and 15.

$$\theta(\omega) = \tan^{-1}\left(\frac{\left|x_i(\omega) - x_j(\omega)\right|}{L}\right) \quad \textbf{(14)}$$

$$x(\omega) = \left|x_i(\omega)\right| - R_{Pi} \cdot \sin(\theta(\omega)) = \left|x_j(\omega)\right| + R_{Pj} \cdot \sin(\theta(\omega)) \quad \textbf{(15)}$$

In Equations 14 and 15, *L* is the length of the beam and the variables R_{Pi} and R_{Pj} represent the distances from the center of rotation to accelerometers A and B respectively. It is only for the two degree of freedom system shown in Figure 2.1 that these relationships will hold true. This means that a system with more degrees of freedom will require this sort of relationship development for every direction being investigated.

The example quadrature spectra plot shown in Figure 3.1 also provides information showing which of the frequencies correspond to each degree of motion. This is shown by the direction of the motion at each point. At the lower frequency, the directions of motion for the two points are opposite, out of phase, proving that the lower frequency is the natural frequency of the rotational mode. The directions of motion of both points are in the positive direction at the

higher frequency, in phase, so it can be said that this frequency is the natural frequency of the translational mode. If the measurements from the example frequency response of Figure 3.1 were used to describe the system of Figure 2.1, for demonstration purposes, the mode shape and frequency matrices would then be as shown in Equation 16.

$$\boldsymbol{\Omega}^2 = \begin{bmatrix} (2\pi f_1)^2 & 0 \\ 0 & (2\pi f_2)^2 \end{bmatrix} \qquad \mathbf{U} = \begin{bmatrix} x(\omega_1) & x(\omega_2) \\ \theta(\omega_1) & \theta(\omega_2) \end{bmatrix} = \begin{bmatrix} 1 & 0 \\ 0 & 1 \end{bmatrix} \qquad \textbf{(16)}$$

In this case the normalized mode shape matrix, **U**, was calculated to be equal to the identity matrix which will happen if there is no coupling between the stiffness terms. What this means to the physical system is that if the system experiences translational motion it will not necessarily rotate as a result. Given the mass matrix of the system based on measurements, the stiffness matrix of the system could then calculated by substituting the mass, frequency, and mode shape matrices into Equation 12.

3.1.2 Results from Experiment

From the measured data, the imaginary parts of the frequency response plots were created for each of the six configurations so that the resonant frequencies could be determined and the mode shapes could be calculated from the acceleration measurements at these frequencies. The quadrature spectra plots for the first three configurations show similarities in shape and Figure 3.2 shows the response plot measured for configuration 1.

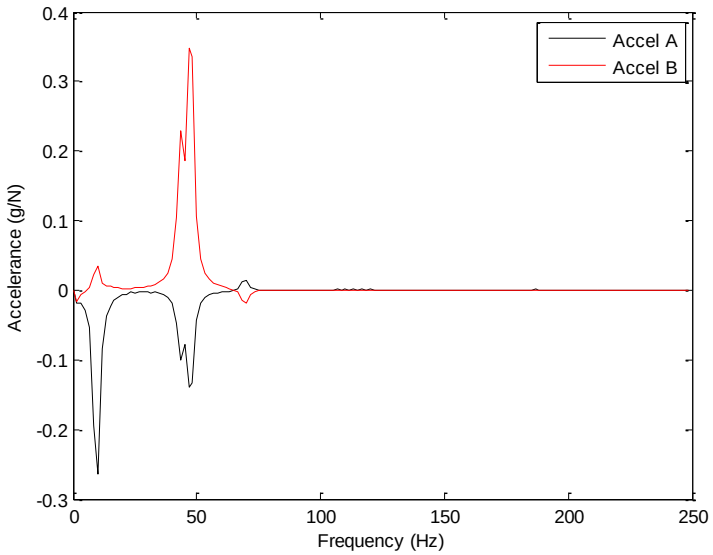

Figure 3.2: Imaginary Part of Frequency Response Plot for Experimental Configuration 1

From Figure 3.2, the natural frequencies of the system can be determined without difficulty, as the two frequencies that the motion peaks at are easily identifiable. The two frequencies are taken to be 10 Hz (62.8 radians per second) and 47 Hz (295.3 radians per second). At 10 Hz the acceleration values are measured to be -0.265 and 0.022 for accelerometers A and B respectively. Likewise at 47 Hz the measurements are -0.138 for accelerometer A and 0.347 for accelerometer B. This frequency response shows that for this system there will be coupling in the stiffness properties. This can be seen from the motions of the points being in opposite directions at each resonant frequency as opposed to the motions seen in Figure 3.1. Using Equations 14 and 15 with the proper values for R_{Pi} and R_{Pj} in configuration 1, the mode shapes are solved for and the resulting frequency and mode shape matrices are shown in Table 3.1.

Table 3.1: Frequency and Mode Shape Matrices for Configuration 1

Frequency Matrix	Mode Shape Matrix
$\boldsymbol{\lambda} = \begin{bmatrix} \omega_1^2 & 0 \\ 0 & \omega_2^2 \end{bmatrix} = \begin{bmatrix} 87208 & 0 \\ 0 & 3948 \end{bmatrix}$	$\mathbf{V} = \begin{bmatrix} x(\omega_1) & x(\omega_2) \\ \theta(\omega_1) & \theta(\omega_2) \end{bmatrix} = \begin{bmatrix} -3.2 & 4.3 \\ 18.2 & 238.5 \end{bmatrix}$

With the mass of the beam, measured with a scale or estimated from the density and volume, the inertia can be solved for and the mass matrix, **M**, can be created using Equation 4. **M**, **U**, and $\boldsymbol{\Omega}^2$ can then be used in Equation 12 to solve for the stiffness matrix of configuration 1 resulting in a two by two matrix similar to that as shown in Equation 17.

$$\mathbf{K} = \mathbf{M} \cdot \mathbf{U} \cdot \boldsymbol{\Omega}^2 \cdot \mathbf{U}^{-1} = \begin{bmatrix} k_{x,x}\left(\frac{N}{m}\right) & k_{x,\theta}\left(\frac{N}{rad}\right) \\ k_{\theta,x}\left(\frac{N}{rad}\right) & k_{\theta,\theta}\left(\frac{N \cdot m}{rad}\right) \end{bmatrix} \quad \textbf{(17)}$$

The resulting stiffness matrix is shown in Table 3.2. The units shown are consistent in every stiffness matrix, **K**, so they will be excluded in further results.

This derived stiffness matrix can be compared to the theoretical stiffness matrix calculated from Equation 4, also shown in Table 3.2.

Table 3.2: Stiffness Matrices for Configuration 1 Calculated Using the Resonant Method

	Theoretical	Measured
Configuration 1	$\mathbf{K} = \begin{bmatrix} 87600 & 9735 \\ 9735 & 1131 \end{bmatrix}$	$\mathbf{K} = \begin{bmatrix} 244030 & 4150 \\ 10230 & 280 \end{bmatrix}$

Comparing the two stiffness matrices, differences are evident but some similarities can be observed. While the values in the measured stiffness matrix are significantly different than the theoretical values, the orders of magnitude of each individual term in the measured stiffness matrix are similar to the orders of magnitude of the corresponding theoretical values.

Similar results are observed from configurations 2 and 3. The quadrature spectra plots for configurations 2 and 3 are shown in Figure 3.3 and Figure 3.4 respectively.

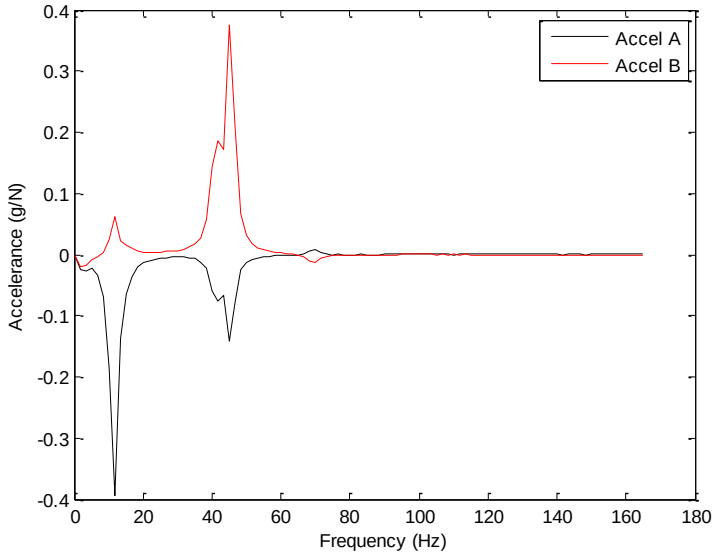

Figure 3.3: Imaginary Part of Frequency Response Plot for Experimental Configuration 2

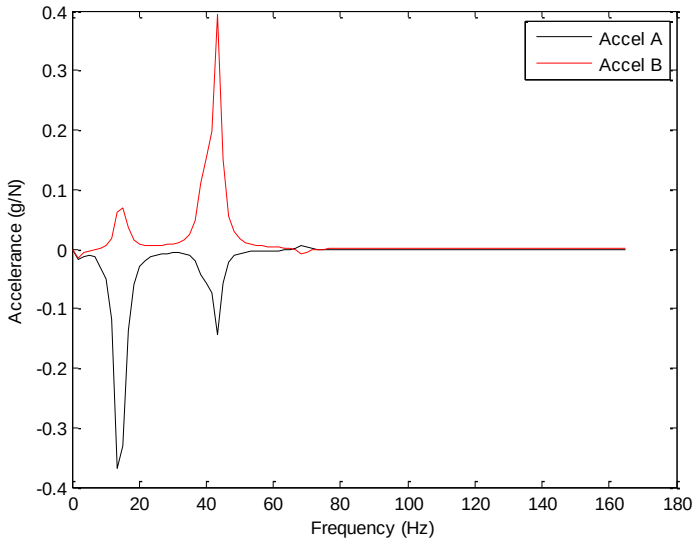

Figure 3.4: Imaginary Part of Frequency Response Plot for Experimental Configuration 3

Using Figure 3.3 and the geometric arrangement of configuration 2 the calculated stiffness matrix and the theoretical stiffness matrix are determined and are shown in Table 3.3 along with the stiffness matrices determined for configuration 1. The same is done for configuration 3 using Figure 3.4 and the resulting stiffness matrices are also shown in Table 3.3.

Table 3.3: Stiffness Matrices for Configurations 1-3 Calculated Using the Resonant Method

	Theoretical	Measured
Configuration 1	$\mathbf{K} = \begin{bmatrix} 87600 & 9735 \\ 9735 & 1131 \end{bmatrix}$	$\mathbf{K} = \begin{bmatrix} 244030 & 4150 \\ 10230 & 280 \end{bmatrix}$
Configuration 2	$\mathbf{K} = \begin{bmatrix} 87600 & 8622 \\ 8622 & 965 \end{bmatrix}$	$\mathbf{K} = \begin{bmatrix} 228760 & 2770 \\ 9800 & 260 \end{bmatrix}$
Configuration 3	$\mathbf{K} = \begin{bmatrix} 87600 & 7510 \\ 7510 & 856 \end{bmatrix}$	$\mathbf{K} = \begin{bmatrix} 197950 & 4050 \\ 8870 & 360 \end{bmatrix}$

Comparing the values calculated for stiffness to the theoretical values in configurations 2 and 3, some of the quantities closely resemble the theoretical values and again all of the orders of magnitude are in agreement with what is expected. Looking at the trends in stiffness values as the springs are separated by greater distances, the values for most terms are expected to decrease with the exception of the one value that remains constant. Looking at the measured stiffness values however, this trend is not realized as some of the values in configuration 3 are higher than in either of the other configurations.

For configurations 4 through 6, the imaginary parts of the frequency response plots more closely resemble the example quadrature spectra plot of Figure 3.1 where the motions were equal at one resonant frequency and equal but opposite in direction at the other. The imaginary component of the frequency response plot for configuration 4 is shown in Figure 3.5.

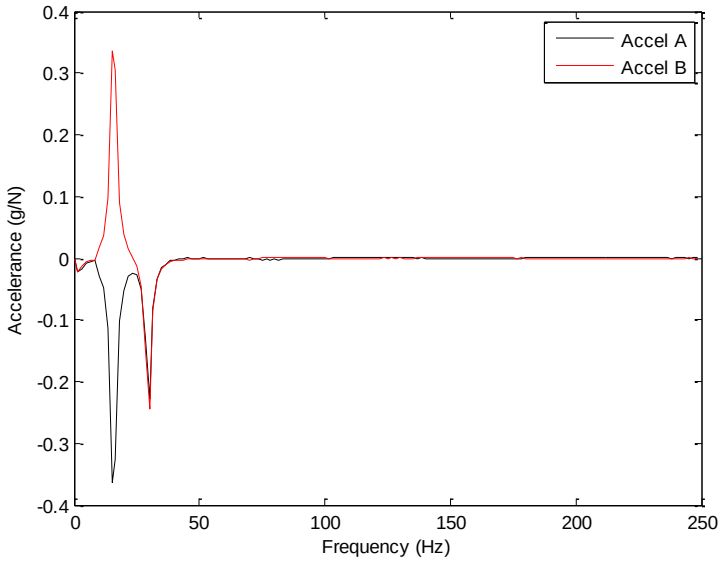

Figure 3.5: Imaginary Part of Frequency Response Plot for Experimental Configuration 4

From Figure 3.5, the resonant frequencies for the system of configuration 4 are measured to be 15 Hz (94.2 radians per second) and 30 Hz (188.5 radians per second). At 15 Hz the

acceleration values are measured to be -0.335 and 0.335 for accelerometers A and B respectively. At 30 Hz the measurements are -0.245 for both accelerometer A and accelerometer B. Again the mode shapes are determined using Equations 14 and 15 with the proper values for R_{Pi} and R_{Pj}, and the frequency and mode shape matrices are shown in Table 3.4.

Table 3.4: Frequency and Mode Shape Matrices for Configuration 4

Frequency Matrix	Mode Shape Matrix
$\boldsymbol{\lambda} = \begin{bmatrix} \omega_1^2 & 0 \\ 0 & \omega_2^2 \end{bmatrix} = \begin{bmatrix} 35531 & 0 \\ 0 & 8883 \end{bmatrix}$	$\mathbf{V} = \begin{bmatrix} x(\omega_1) & x(\omega_2) \\ \theta(\omega_1) & \theta(\omega_2) \end{bmatrix} = \begin{bmatrix} 6.9 & 0 \\ 0 & 247.5 \end{bmatrix}$

These frequency and mode shape matrices are used along with the mass matrix in Equation 12 to solve for the stiffness matrix of configuration 4. The calculated stiffness matrix is shown along with the theoretical stiffness matrix, again determined from Equation 4, in Table 3.5. In configuration 4 there will still exist all the potential causes for error as were present in configuration 1 but in this case the measured stiffness matrix more closely resembles the theoretical values. The stiffness matrix calculated for configuration 4 shows no coupling between the different directions and this is verified in observing the geometry of the system as well as the frequency response plot. The only way in which the frequency response plot of the system will match that of the example schematic shown in Figure 3.1 is if the system has no coupling between the different motions. In configuration 4 the center of rotation will coincide with the center of mass due to the locations of the springs and this is why there are no coupled terms in the stiffness matrix.

Configurations 5 and 6 also have no coupling terms, due to similar geometry, and the quadrature spectra plots are shown in Figure 3.6 and Figure 3.7 respectively.

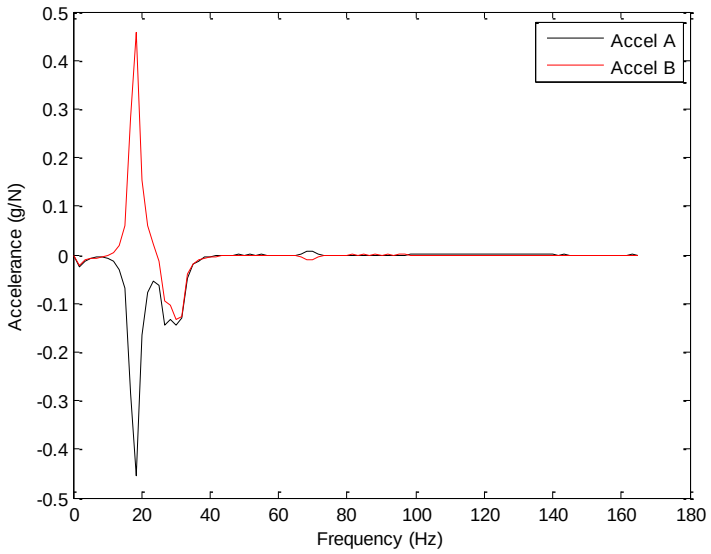

Figure 3.6: Imaginary Part of Frequency Response Plot for Experimental Configuration 5

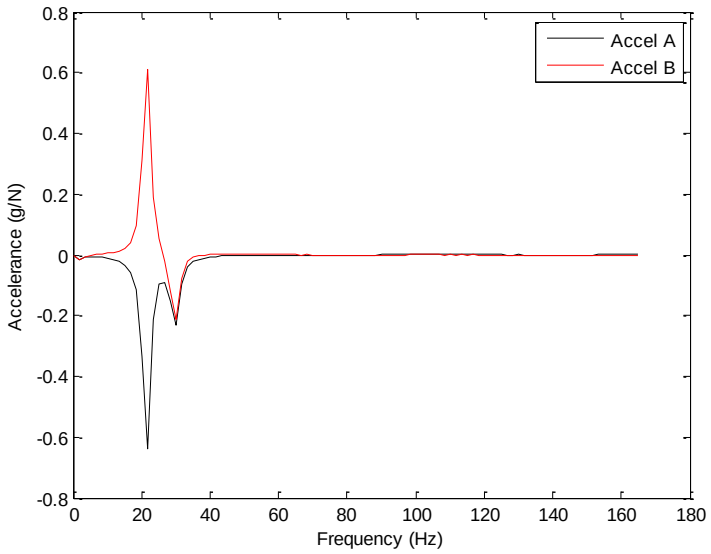

Figure 3.7: Imaginary Part of Frequency Response Plot for Experimental Configuration 6

The stiffness matrices were calculated for configurations 5 and 6 both theoretically and based off measurements and these are also shown in Table 3.5.

Table 3.5: Stiffness Matrices for Configurations 4-6 Calculated Using the Resonance-Based Method

	Theoretical	Measured
Configuration 4	$\mathbf{K} = \begin{bmatrix} 87600 & 0 \\ 0 & 50 \end{bmatrix}$	$\mathbf{K} = \begin{bmatrix} 109000 & 0 \\ 0 & 210 \end{bmatrix}$
Configuration 5	$\mathbf{K} = \begin{bmatrix} 87600 & 0 \\ 0 & 117 \end{bmatrix}$	$\mathbf{K} = \begin{bmatrix} 109000 & 0 \\ 0 & 310 \end{bmatrix}$
Configuration 6	$\mathbf{K} = \begin{bmatrix} 87600 & 0 \\ 0 & 212 \end{bmatrix}$	$\mathbf{K} = \begin{bmatrix} 109000 & 0 \\ 0 & 460 \end{bmatrix}$

The trends in the values of the stiffness matrices measured as the springs are separated by increasingly large distances, match the trends realized in the theoretical stiffness matrices. As the distance between the springs increases, the stiffness value in the *x* direction remains constant while the stiffness value in the θ direction increases. The measured stiffness values representing the coupled terms are also zero in all three configurations, matching those of the theoretically calculated values.

3.1.3 Resonant Method Analysis

There are a number of reasons for the discrepancies between the calculated and theoretical stiffness matrices including the participation of coupled off-axis modes as well as inaccuracies in experimental setup. Due to the way in which the springs are attached to the suspended mass, there will be multi-dimensional coupling between the different translational modes. So while the one translational mode (x) is the target for measurement, the modes in other directions (y and z), which occur at the same frequency, will be excited and this will introduce error into the frequency response data. Because of these imperfections in the frequency response

results, the resonant frequencies and mode shapes of the system will be measured inaccurately. The experimental setup also introduces a degree of uncertainty both in assumptions made and the measurements taken. In assuming that the center of rotation is the elastic center of the system, if the actual center of rotation is slightly different than this point, that little bit of error will be introduced into the multiple equations using this measurement. Another assumption that may cause error is the assumption that the spring forces can be modeled at a point despite the circular base of the spring. Also as with any experiment, there is some error introduced in exciting the system and taking the measurements. These measurement errors are responsible for the lack of symmetry between the off-diagonal terms of the calculated stiffness matrix. While some of these sources of error are unavoidable, others offer opportunity for refinement in other works. The true center of rotation, for example, can be determined using computational analysis and this will eliminate that error as well as provide an insight into how the center of rotation varies along the length of the beam as the beam is in motion.

Using the geometric information for each configuration, the theoretical stiffness and mass matrices were determined for all six experimental configurations using Equation 4. The theoretical eigenvalues for each system were then mathematically derived using Equation 10 and the frequencies obtained are shown in Table 3.6 where they are compared to the frequencies measured for each configuration from the frequency response plots. The measured frequencies are also plotted against the theoretically derived frequencies in Figure 3.8 and a best fit line shows that the correlation in the measurements is 91.4 percent.

Table 3.6: Measured and Theoretical Frequencies of Two Degree of Freedom System Measured From Frequency Response Plots

Experiment Configuration	Direction	Theoretical Frequencies (Hz)	Measured Frequencies (Hz)
1	Translation (x)	54.0	47
	Rotation (θ)	5.54	10
2	Translation (x)	51.0	45
	Rotation (θ)	9.0	12
3	Translation (x)	48.3	43
	Rotation (θ)	12.8	13
4	Translation (x)	33.3	30
	Rotation (θ)	8.98	15
5	Translation (x)	33.3	30
	Rotation (θ)	13.8	18
6	Translation (x)	33.3	30
	Rotation (θ)	18.6	22

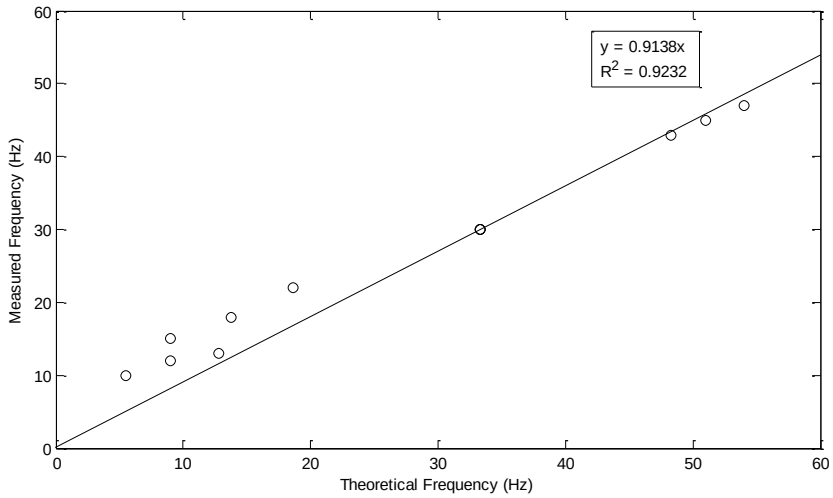

Figure 3.8: Correlation Plot between Measured and Theoretical Frequencies

Sensitivity calculations were performed to realize the degree to which the resonant frequencies of the system would change with slight differences in experimental measurements. The variables under investigation were the mass and inertia of the beam, the distance between the center of gravity and the center of rotation, and the stiffness of each of the four springs. The calculations were performed by varying each variable by ten percent about a nominal value,

while keeping the other variables at their respective nominal value. The effects on both the lower and higher resonant frequencies are shown in Figure 3.9 and Figure 3.10 respectively.

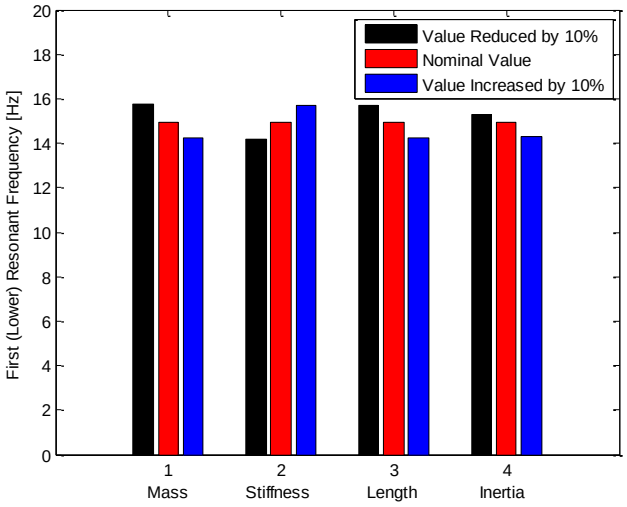

Figure 3.9: Sensitivity Plot for Lower Resonant Frequency

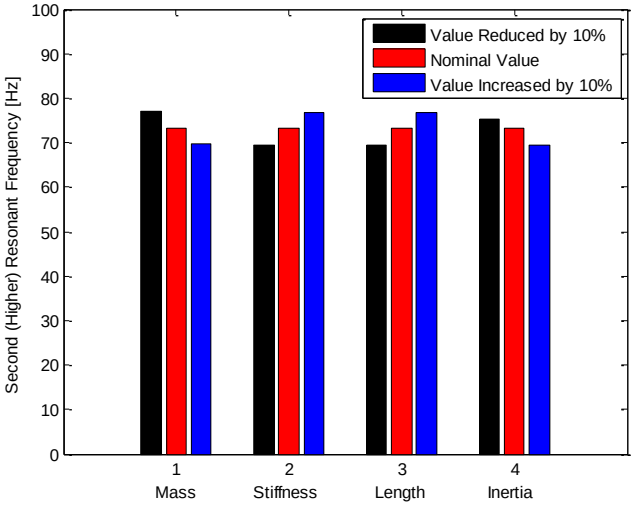

Figure 3.10: Sensitivity Plot for Higher Resonant Frequency

From these sensitivity plots, the effects of small errors in measurement are observed in the resultant variations in calculated resonant frequencies. The effects of these small sources of error are only shown for the resonant frequencies but as these values are used in the stiffness

matrix determination, it is seen how these errors would compound causing significant differences between experimentally measured and theoretically calculated stiffness values. Based on the sensitivity data and the comparisons between measured and calculated stiffness values, one possible source of error might be in the measuring of the stiffness of each spring. If the spring constant for each spring was higher than measured, many terms in the measured stiffness matrices would be higher than the theoretically calculated values, as is seen in many cases. This effect would also be seen if the dynamic stiffness of the spring was higher than the measured static value.

Through conducting this experiment, it has been shown that a unique stiffness matrix for the system can, to a certain degree, be measured using this resonant method of calculation. The individual terms determined for the stiffness matrices matched the theoretical values in their order of magnitude but differed greatly in value. There are many plausible sources of error, as a few were discussed, and the effects of small measurement errors were shown through sensitivity calculations. For the systems in which there was no coupling between the different directions, the calculated stiffness values were measured to be relatively similar to the theoretical values and the same trends were observed as the distance between the springs was varied. In viewing the results, this method of measuring multi-directional stiffness values requires a great degree of accuracy in the experimental setup as small errors in configuration can propagate into large inaccuracies in the measured stiffness matrix. It is also important to remember that for higher degree of freedom systems, the relationships between the measured acceleration data and the desired mode shapes will become more complicated and might not be able to be determined for all systems.

3.2 Frequency Response Method

3.2.1 Method Description

The second method that was investigated uses relative acceleration data at a pivot point to determine the stiffness of a joint [7]. This method uses acceleration measurements at many frequencies and does not require resonance data. Previous research has shown that this method can theoretically be used to calculate a multi-directional stiffness matrix of a system using measured accelerance data but this lacks experimental validation. This method can be explained by evaluating the two degree of freedom system and the stiffness matrix of the system can then be calculated from the accelerance data obtained from the experiment. Figure 3.11 shows the two degree of freedom system with the pivot point *P* and the relative accelerations at points *i* and *j* located at the accelerometers.

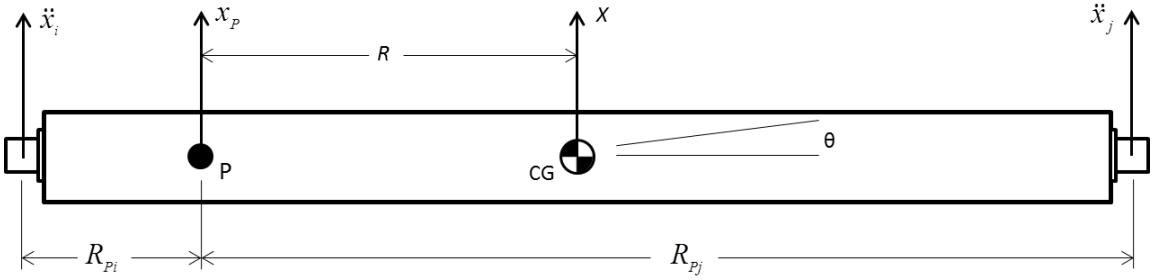

Figure 3.11: Two Degree of Freedom System Used with Frequency Response Method

For any system, the acceleration data is obtained at a number of points and then transformed to represent acceleration data at the pivot point. Equation 18 shows the relationships between the motions at points *i* and *j* and the motion at the pivot point *P*.

$$\left[\ddot{x}_i\right] = \begin{bmatrix} 1 & -R_{pi} \end{bmatrix} \begin{bmatrix} \ddot{x}_p \\ \ddot{\theta}_p \end{bmatrix} \qquad \left[\ddot{x}_j\right] = \begin{bmatrix} 1 & R_{pj} \end{bmatrix} \begin{bmatrix} \ddot{x}_p \\ \ddot{\theta}_p \end{bmatrix} \qquad \textbf{(18)}$$

It is important to notice the direction of the distance measurements and to keep the sign in agreement with the coordinate axis used. The acceleration data for each point is then combined and the transformation matrix is defined as shown in Equation 20. This equation describes the two degree of freedom system but similar equations can be applied to systems with higher degrees of freedom.

$$\begin{bmatrix} \ddot{x}_i \\ \ddot{x}_j \end{bmatrix} = \begin{bmatrix} 1 & -R_{pi} \\ 1 & R_{pj} \end{bmatrix} \begin{bmatrix} \ddot{x}_p \\ \ddot{\theta}_p \end{bmatrix} \quad \textbf{(19)}$$

$$\mathbf{T} = \begin{bmatrix} 1 & -R_{pi} \\ 1 & R_{pj} \end{bmatrix} \qquad \ddot{\mathbf{X}}_{\mathbf{P}} = \begin{bmatrix} \ddot{x}_p \\ \ddot{\theta}_p \end{bmatrix} \quad \textbf{(20)}$$

$$\begin{bmatrix} \ddot{x}_i \\ \ddot{x}_j \end{bmatrix} = \mathbf{T} \cdot \ddot{\mathbf{X}}_{\mathbf{P}} \quad \textbf{(21)}$$

Equation 21 can then be solved for the acceleration data at the pivot point by taking the pseudo-inverse of the transformation matrix as shown in Equation 22.

$$\ddot{\mathbf{X}}_{\mathbf{P}} = [\mathbf{T}]^{+} \cdot \begin{bmatrix} \ddot{x}_i \\ \ddot{x}_j \end{bmatrix} \quad \textbf{(22)}$$

With the acceleration data for the pivot point, the stiffness matrix can then be calculated using a combination of Newton's second law and frequency domain transformations. Summing the forces and moments of the system shown in Figure 3.11, the reaction force vector, **F**, at the pivot point can be related to the accelerations at the pivot points by Equation 23 where the moment of inertia term is the moment of inertia about the pivot point after applying the parallel axis theorem.

$$\mathbf{F} = \begin{bmatrix} F_x \\ M_z \end{bmatrix} = \begin{bmatrix} m & -mR \\ -mR & I_P \end{bmatrix} \cdot \ddot{\mathbf{X}}_{\mathbf{P}} \quad \textbf{(23)}$$

With the force matrices solved for, the equation relating the force and the relative displacement matrices can be used to solve for the stiffness. Because only acceleration values are measured, the displacement values must be calculated from these acceleration measurements. This is done by transforming the acceleration data points into the frequency domain and solving for the displacements similar to what was done in Equation 13 as shown in Equation 24.

$$\mathbf{X_P}(\omega) = \begin{bmatrix} \mathbf{X_P}(\omega) \\ \boldsymbol{\theta}_\mathbf{P}(\omega) \end{bmatrix} = -\frac{1}{\omega^2}\ddot{\mathbf{X}}_\mathbf{P}(\omega) \qquad \textbf{(24)}$$

These displacements are assumed to be relative displacements due to the rigidity of the base to which the free mass is jointed. With the reaction forces and the relative displacements, the stiffness matrix can be solved for. It is important to notice that the acceleration measurements are taken at multiple frequencies and each of these measurements represent a separate data point. This results in the equation relating the forces and displacements to take the form shown in Equation 25 where *n* is the number of frequencies that measurements are taken.

$$\begin{bmatrix} \mathbf{F}(\omega_1) & \mathbf{F}(\omega_2) & \cdots & \mathbf{F}(\omega_n) \end{bmatrix} = [\mathbf{K}] \cdot \begin{bmatrix} \mathbf{X_P}(\omega_1) & \mathbf{X_P}(\omega_2) & \cdots & \mathbf{X_P}(\omega_n) \end{bmatrix} \qquad \textbf{(25)}$$

$$\left[\hat{\mathbf{F}}(\omega)\right] = [\mathbf{K}]\left[\hat{\mathbf{X}}_\mathbf{P}(\omega)\right] \qquad \textbf{(26)}$$

Equations 25 and 26 assume that the values of the stiffness matrix are independent of frequency which is a limiting assumption associated with this and most other methods. From these equations there are multiple ways in which the stiffness matrix can be solved for depending on the amount of error reduction desired as well as the source of error assumed. The first way to estimate the lower bound (L) stiffness matrix would be to assume that the main source of error resides in the displacement spectra, and to solve for the lower bound of the stiffness matrix. This is done according to Equation 27.

$$[\mathbf{K}]_L = \left\{\left[\hat{\mathbf{F}}(\omega)\right]\cdot\left[\hat{\mathbf{X}}_{\mathbf{P}}(\omega)\right]^{\mathbf{T}}\right\}\cdot\left\{\left[\hat{\mathbf{X}}_{\mathbf{P}}(\omega)\right]\cdot\left[\hat{\mathbf{X}}_{\mathbf{P}}(\omega)\right]^{\mathbf{T}}\right\}^{-1} \quad \textbf{(27)}$$

The upper bound (U) stiffness matrix can be estimated by assuming that the error is generated from the force spectra and this will result in an upper bound stiffness matrix as shown in Equation 28.

$$[\mathbf{K}]_U = \left\{\left[\hat{\mathbf{F}}(\omega)\right]\cdot\left[\hat{\mathbf{F}}(\omega)\right]^{\mathbf{T}}\right\}\cdot\left\{\left[\hat{\mathbf{X}}_{\mathbf{P}}(\omega)\right]\cdot\left[\hat{\mathbf{F}}(\omega)\right]^{\mathbf{T}}\right\}^{-1} \quad \textbf{(28)}$$

3.2.2 Results from Experiment

From the experiment conducted on the two degree of freedom system, accelerance data was collected at two different points over a range of 512 different frequencies between zero and 851 Hz. This method only requires measurements at a certain number of frequencies, equal to the number of degrees of freedom. However the calculations allow the use of all the data from every frequency and the measurement errors can theoretically be minimized by utilizing the extra data. By using the measurements at more frequencies, the system is effectively being over-determined and so the error in the data should be mitigated. For this reason, many of the accelerance measurements were used in the calculations but only the measurements taken at frequencies below 100 Hz were used. The data at the higher frequencies was not used to avoid the frequencies at which the flexural modes of the beam would become present as this would introduce new sources of error. The flexural modes of a steel beam would occur at much higher frequencies than the 100 Hz but caution was heeded.

For each of the experimental configurations, the procedure was followed in converting the acceleration measurements from the locations of the accelerometers to acceleration data at

the pivot point. The inertial matrices were then determined based off geometry and used with the acceleration data to determine the force matrices. With the forces and the derived displacements, the stiffness matrices were calculated using Equations 27 and 28. These calculations were performed using computational analysis (Matlab) due to the large number of data readings. Table 3.7 shows the calculated stiffness matrices for each configuration along with the theoretical stiffness matrices, shown for comparison.

Table 3.7: Stiffness Matrices Calculated Using the Frequency Response Method

	Theoretical	Lower Bound	Upper Bound
Configuration 1	$\mathbf{K}=\begin{bmatrix}87600 & 9735\\ 9735 & 1131\end{bmatrix}$	$\mathbf{K}_{L,1}=\begin{bmatrix}100210 & 4490\\ 1600 & 970\end{bmatrix}$	$\mathbf{K}_{U,1}=\begin{bmatrix}142620 & 10820\\ 7070 & 2170\end{bmatrix}$
Configuration 2	$\mathbf{K}=\begin{bmatrix}87600 & 8622\\ 8622 & 965\end{bmatrix}$	$\mathbf{K}_{L,2}=\begin{bmatrix}95040 & 3438\\ 1611 & 794\end{bmatrix}$	$\mathbf{K}_{U,2}=\begin{bmatrix}138280 & 8370\\ 4110 & 1630\end{bmatrix}$
Configuration 3	$\mathbf{K}=\begin{bmatrix}87600 & 7510\\ 7510 & 856\end{bmatrix}$	$\mathbf{K}_{L,3}=\begin{bmatrix}80484 & 2048\\ 4260 & 662\end{bmatrix}$	$\mathbf{K}_{U,3}=\begin{bmatrix}88241 & 3604\\ 4057 & 970\end{bmatrix}$
Configuration 4	$\mathbf{K}=\begin{bmatrix}87600 & 0\\ 0 & 50\end{bmatrix}$	$\mathbf{K}_{L,4}=\begin{bmatrix}113430 & 110\\ 260 & 260\end{bmatrix}$	$\mathbf{K}_{U,4}=\begin{bmatrix}147170 & 570\\ 1710 & 320\end{bmatrix}$
Configuration 5	$\mathbf{K}=\begin{bmatrix}87600 & 0\\ 0 & 117\end{bmatrix}$	$\mathbf{K}_{L,5}=\begin{bmatrix}111230 & 200\\ 500 & 310\end{bmatrix}$	$\mathbf{K}_{U,5}=\begin{bmatrix}147730 & 910\\ 1960 & 370\end{bmatrix}$
Configuration 6	$\mathbf{K}=\begin{bmatrix}87600 & 0\\ 0 & 212\end{bmatrix}$	$\mathbf{K}_{L,6}=\begin{bmatrix}107950 & 100\\ 400 & 430\end{bmatrix}$	$\mathbf{K}_{U,6}=\begin{bmatrix}132820 & 420\\ 1640 & 500\end{bmatrix}$

3.2.3 Frequency Response Method Analysis

This experiment has proven that a unique stiffness matrix of the two degree of freedom system can also be measured with this method of calculation using the pivot point. Again the orders of magnitude for most terms are in agreement between the measured and theoretical values and some theoretical terms are within the range between the upper and lower bound values of the corresponding measured stiffness matrices. It can also be seen in Table 3.7 that

many of the same trends are seen between measured and theoretical values as the distance between the springs is increased.

Despite these similarities between measured and calculated values, there are still significant differences between the two. Perhaps the most important thing to notice is the difference between the upper and lower bounds of the measured stiffness matrices. These large differences demonstrate the effects of error in the measurements. If there was zero error in both the displacement and force matrices derived, then the upper bound stiffness matrix would be equal to the lower bound stiffness matrix. Because that is not the case and there is instead a large difference between the two values, as seen in Table 3.7, there must be error in the measurements causing these differences. Another notable difference is observed in comparing the off-diagonal terms of the stiffness matrices for configurations 4-6. Using this method, the measured stiffness matrices show that there is some coupling between the two degrees of motion in these three configurations, which theoretically there should not be. The off-diagonal terms are however very low, representing only a small amount of coupling.

The same sources of error discussed previously would still have an effect on the calculated stiffness values determined with this method but the effects of measurement errors would be different as the resonant frequencies are not determined with this method. Again the coupled axial modes will be excited due to symmetry and this will contribute to uncertainty in the accelerance data measured. The results from these calculations and measurements also show that the measured spring constant might be lower than the actual spring constant as many of the measured stiffness values are higher than the theoretical values. Also the non-symmetric off-diagonal terms show either errors in measurement or eccentricities at the joint.

Chapter 4: Conclusions

4.1 Conclusions about Procedures

Each of the methods that were examined successfully produced a unique stiffness matrix for the experimental two degree of freedom system but the estimated values were not consistent with the theoretically determined stiffness matrices. The effects of some of the measurement errors associated with geometry, mass, and spring constants of the system were observed in the sensitivity plots of Figure 3.9 and Figure 3.10. There are other sources of error that deal with assumptions made in creating the experiment.

The springs used were compression springs with an outside diameter of 1.375 inches (0.0349 m) and it was assumed that the springs would exhibit symmetrical properties allowing the force components to be modeled as a point load. However with the diameter of the springs being large, relative to the dimensions of the experimental setup, the spring might demonstrate asymmetrical properties as it is not applying a force at a point but rather over an area. The springs were also arranged identically in each experimental test to ensure consistent preloading of the springs. This was done by measuring the deflection of the springs before conducting each test, but if the springs were preloaded differently in some cases the results would not be consistent throughout. Another assumption that was made regarding the springs was that the static stiffness would be a reasonable approximation for the stiffness experienced in a dynamic experiment. If the dynamic stiffness of the springs was actually higher than the static stiffness though, the measured stiffness matrices of the system would consist of higher values than what was theoretically calculated, as was seen in many of the results.

Another source of error originates from the simplification of the experiment in modeling the beam and springs as a two degree of freedom system. An assumption made about the system is that there is no modal participation from other resonances but this may not be the case. If the other modes do participate and this motion is not accounted for, there will be inaccuracies in the measured acceleration data. This effect will be especially significant if the modes are closely spaced, i.e. the corresponding frequencies are approximately equal. The effect that this sort of error would have on the final stiffness values would be dependent on many factors including whether the erroneous mode was at a slightly higher or slightly lower frequency. The effects would also depend on the direction of motion in which the mode contributed resulting in measured values with either a greater or a smaller magnitude.

Previously mentioned was the assumption that the system must either be lightly damped or proportionally damped to apply the methods used in calculating stiffness. Because the system consisted of only a rigid steel beam and compression springs, it was assumed that the system would exhibit a very small amount of damping. However, if the damping of the system was underestimated and this effect was not taken into account, the damping would contribute to erroneous measurements both in the resonant frequencies as well as the final stiffness values. Using the resonance-based method, the resonant frequencies were measured and used in calculating the stiffness matrix values. These resonant frequencies are used as the natural frequencies of the system but if there is significant damping these frequencies could be quite different from the natural frequency values. The natural frequency would be the resonant frequency of a purely undamped system but because there is damping in every system, the measured resonant frequencies are actually the damped natural frequencies. With lightly damped systems, there is not a large difference between these two frequency values but if the damping in

the experimental system is significantly high, the measured frequency might be noticeably less than the actual natural frequency. Another effect that the underestimation of damping would cause is the way in which the stiffness matrix of the system would then include the effects of damping. This would result in an overestimation of the stiffness matrix values as they would include both stiffness and damping effects. The use of linear springs results in the simplifying assumption that the system can be modeled as lightly damped, but the overestimations in the calculated stiffness matrices might suggest otherwise.

Though neither calculation method successfully measured the same stiffness values as were derived theoretically, both were proven capable of approximating a unique stiffness matrix for the two degree of freedom system tested, at least to similar orders of magnitude. It is important to note that throughout industry, the stiffness properties of bushings in many directions are neither known nor reported. Thus any method that can be used to estimate the multi-directional stiffness matrix of a bushing would considerably improve industrial practice in choosing bushings for certain applications. Also with the precision measurement systems that have been developed, the amount of error in measurements can be minimized and would undoubtedly improve upon the measurement process used in determining the stiffness matrix using either of the two methods examined.

4.2 Recommendations for Future Work

Due to some simplifications made in the experiment, there are natural extensions to this problem that may be investigated in future work. The first of which would be to extend the scope of the problem to include higher order systems. The bushing, as discussed, is modeled in all six degrees of freedom so if the two methods were applied in calculating the stiffness of a six degree of freedom system this would provide further insight into the feasibility of using either method,

or perhaps even both methods, in measuring the stiffness matrix of an actual bushing. A step further than this would then be to apply the same methods to multiple bushings in series. This would have practical application as suspension systems often consist of multiple bushings and determining the effects of each bushing on that system would allow for better modeling of the entire system.

Additional works might also try and address ways in which to reduce the amount of error that was experienced in measurements. One way in which to accomplish this might be to better classify the system being tested by either using narrow springs to ensure symmetry or to measure the dynamic stiffness of the springs themselves. The system can also be modeled more accurately by determining the actual center of rotation as the system is oscillating. Another way in which to reduce the amount of error in the system would be to address the damping issue. If a way in which to control the source of damping could be used such that the effective damping ratio could be known, the effects of damping could be investigated. This type of study would provide insight as to whether or not these methods can be used when there is damping in the system.

In comparing the two methods, each has advantages and disadvantages. The resonance measurement based method did seem to effectively measure the stiffness properties of the uncoupled systems of configurations 4-6 and the measured stiffness matrices accurately showed the lack of coupling. This method of calculation however involves many steps in determining the relationships between the directions of motion and in measuring the resonant frequencies and accelerations from the frequency response plots. While these steps were not too time consuming for the simple two degree of freedom system used, when performing tests on a six degree of freedom system, these steps will require more time and may prove impossible to solve. Using the

resonance based method might prove more accurate if the system can be geometrically determined to have no coupling between the different directions of motion.

The measured stiffness matrices from the pivot point method, on the other hand, failed to show the lack of coupling between the directions of motion for configurations 4-6. However the values for the stiffness matrices calculated were considerably closer to the theoretically calculated values. The steps taken in solving for the stiffness matrix using the pivot point method are also more direct and are based upon using the actual measurements as opposed to taking readings from plots of the data. Based on the higher degree of accuracy in measurement as well as the time advantage using the pivot point method and the correct modeling of uncoupled systems using the resonance based method, perhaps a hybrid of the two methods could be investigated to minimize the amount of error in measurement.

REFERENCES

[1] MTS Systems Corporation. *Accurate and Affordable Bushing Durability Test*. Web. 9 Mar. 2010. <http://www.mts.com/en/Material/Dynamic/index.asp>.

[2] Garcia, Maria-Jose. *Engineering Rubber Bushing Stiffness Formulas including Dynamic Amplitude Dependence*. Master's Thesis. Royal Institute of Technology, Stockholm, 2006.

[3] Barber, Andrew J. *Accurate Models for Bushings and Dampers Using the Empirical Dynamics Method*. Tech. MTS Systems Corporation.

[4] Gil-Negrete, N., J. Vinolas, and L. Kari. "A Simplified Methodology to Predict the Dynamic Stiffness of Carbon-black Filled Rubber Isolators Using a Finite Element Code." *Journal of Sound and Vibration* 296 (2006): 757-76.

[5] Sohn, Jeong-Hyun, Seung-Kyu Lee, Jin-Kyu Ok, and Wan-Suk Yoo. "Comparison of Semi-Physical and Black-Box Bushing Model for Vehicle Dynamics Simulation." *Journal of Mechanical Science and Technology* 21 (2007): 264-71.

[6] Wolf, Susann, Joachim Haase, Christoph Claub, Michael Jockel, and Jurgen Losch. *Methods of Sensitivity Calculation Applied to a Multi-Axial Test Rig for Elastomer Bushings*. Thesis. Fraunhofer-Institute for Integrated Circuits, 2008.

[7] Lim, T.C., and R. Singh. "Vibration Transmission Through Rolling Element Bearings, Part I: Bearing Stiffness Formulation" *Journal of Sound and Vibration* (1990): **139**(2), 179-199.

[8] Wyatt Becker, Patricia J., Robert H. Wynn Jr., Edward J. Berger, and Jason R. Blough. "Using Rigid-Body Dynamics to Measure Joint Stiffness" *Mechanical Systems and Signal Processing* (1999): **13**(5), 789-801.

[9] Meirovitch, Leonard. Fundamentals of Vibrations (2010): *Waveland Press, Inc*.

APPENDIX A: List of Symbols

Symbols

k	spring stiffness [N/m]
O	center of gravity
P	center of rotation / elastic center
R	distance from center of gravity to center of rotation [m]
s	distance from spring to center of rotation [m]
x	translational motion at center of gravity [m]
θ	rotational motion at center of gravity [rad]
F_1	reaction force on spring 1 [N]
F_2	reaction force on spring 2 [N]
I_o	mass moment of inertia of rigid beam about the center of mass [$\mathrm{kg}\cdot\mathrm{m}^2$]
m	mass of rigid beam [kg]
$\mathbf{M}$	mass matrix
$\mathbf{K}$	stiffness matrix
$\mathbf{X}$	mode vector
$\mathbf{x}$	motion matrix
f	frequency [Hz]
ω	angular frequency [rad/s]
$\mathbf{\Omega}^2$	eigenvalue matrix
$\mathbf{V}$	eigenvector matrix
$\mathbf{U}$	normalized eigenvector matrix
x_i	translational motion at accelerometer A [m]
x_j	translational motion at accelerometer B [m]
L	length of rigid beam [m]
R_{Pi}	distance between pivot point and accelerometer A [m]
R_{Pj}	distance between pivot point and accelerometer B [m]
x_P	translational motion at pivot point [m]
θ_P	rotational motion at pivot point [rad]
I_P	mass moment of inertia of rigid beam about the pivot point [$\mathrm{kg}\cdot\mathrm{m}^2$]
F_x	reaction force at pivot point [N]
M_z	reaction moment at pivot point [$N\cdot\mathrm{m}$]
$\mathbf{F}$	reaction force and moment vector matrix
$\mathbf{X}_P$	mode vector at pivot point
$\hat{\mathbf{F}}$	reaction force and moment matrix over a range of excitation frequencies
$\hat{\mathbf{X}}_P$	mode vector at pivot point over a range of excitation frequencies

n	number of frequencies for which measurements are taken
$\mathbf{K}_U$	upper boundary stiffness matrix
$\mathbf{K}_L$	lower boundary stiffness matrix

Superscripts

$\cdot\cdot$	second derivative
-1	inverse
$+$	pseudo-inverse
T	transpose
$\wedge$	estimated

Superscripts

1	pertaining to lower of resonant frequencies
2	pertaining to higher of resonant frequencies
P	about the elastic center of beam
L	lower bound
U	upper bound